MOLECULAR AND CELLULAR BIOLOGY, Mar. 1996, p. 1203–1211 Vol. 16, No. 3
0270-7306/96/$04.00+0

The Recessive Phenotype Displayed by a Dominant Negative Microphthalmia-Associated Transcription Factor Mutant Is a Result of Impaired Nuclear Localization Potential

KIMIKO TAKEBAYASHI,[1] KAZUHIRO CHIDA,[2] IKUYO TSUKAMOTO,[3] EIICHI MORII,[1] HIROSHI MUNAKATA,[4] HEINZ ARNHEITER,[5] TOSHIO KUROKI,[2] YUKIHIKO KITAMURA,[1] AND SHINTARO NOMURA[1]*

Department of Pathology, Osaka University Medical School, Suita, Osaka 565,[1] Department of Cancer Cell Research, Institute of Medical Science, University of Tokyo, Minato-ku, Tokyo 108,[2] Department of Food Science and Nutrition, Nara Women's University, Kitauoyanishi-machi, Nara 630,[3] and Department of Biochemistry, Tohoku University Medical School, Aoba-ku, Sendai, Miyagi 980-77,[4] Japan, and Laboratory of Developmental Neurogenetics, National Institute of Neurological Disorders and Stroke, Bethesda, Maryland 20892[5]

Received 3 July 1995/Returned for modification 22 August 1995/Accepted 26 December 1995

In the DNA binding domain of microphthalmia-associated transcription factor (MITF), four mutations are reported: *mi*, Mi^{wh}, mi^{ew}, and Mi^{or}. MITFs encoded by the *mi*, Mi^{wh}, mi^{ew}, and Mi^{or} mutant alleles (*mi*-MITF, Mi^{wh}-MITF, mi^{ew}-MITF, and Mi^{or}-MITF, respectively) interfered with the DNA binding of wild-type MITF, TFE3, and another basic helix-loop-helix leucine zipper protein in vitro. Polyclonal antibody against MITF was produced and used for investigating the subcellular localization of mutant MITFs. Immunocytochemistry and immunoblotting revealed that more than 99% of wild-type MITF and Mi^{wh}-MITF located in nuclei of transfected NIH 3T3 and 293T cells. In contrast, *mi*-MITF predominantly located in the cytoplasm of cells transfected with the corresponding plasmid. When the immunoglobulin G (IgG)-conjugated peptides representing a part of the DNA binding domain containing *mi* and Mi^{wh} mutations were microinjected into the cytoplasm of NRK49F cells, wild-type peptide and Mi^{wh}-type peptide-IgG conjugate localized in nuclei but *mi*-type peptide-IgG conjugate was detectable only in the cytoplasm. It was also demonstrated that the nuclear translocation potential of Mi^{or}-MITF was normal but that mi^{ew}-MITF was impaired as well as *mi*-MITF. In cotransfection assay, a strong dominant negative effect of Mi^{wh}-MITF against wild-type MITF-dependent transactivation system on tyrosinase promoter was observed, but *mi*-MITF had a small effect. However, by the conjugation of simian virus 40 large-T-antigen-derived nuclear localization signal to *mi*-MITF, the dominant negative effect was enhanced. Furthermore, we demonstrated that the interaction between wild-type MITF and *mi*-MITF occurred in the cytoplasm and that *mi*-MITF had an inhibitory effect on nuclear localization potential of wild-type MITF.

A double gene dose of mutant alleles at the mouse *mi* locus produces various abnormalities of microphthalmia: depletion of pigment in hairs, eyes, and inner ears; deafness; osteopetrosis; and a decrease in the number of mast cells (10, 13, 15, 26, 29, 32, 40, 42, 44, 48, 49). Seventeen mutant alleles have been reported at the *mi* locus (13, 27, 40). The *mi* locus encodes the basic helix-loop-helix leucine zipper (bHLH-ZIP) transcription factor (20, 22), which was termed microphthalmia-associated transcription factor (MITF) (45). Proteins of the bHLH-ZIP family are considered to bind DNA by the basic domain, to dimerize through the helix-loop-helix domain, and to be stabilized by the leucine zipper domain. N-terminal to the DNA binding domain is an amphipathic helix that serves to activate the transcription. Sequence relationships within the bHLH-ZIP proteins clearly show that MITF is most closely related to the transcription factors TFEB, TFEC, and TFE3 (1, 4, 53), all of which can form stable heterodimers with MITF and with each other (19). Specificity of DNA binding is well characterized in bHLH-ZIP proteins; most bHLH-ZIP proteins bind the E-box motif whose consensus sequence is CANNTG. Recently, it was reported that MITF regulates the expression of the tyrosinase gene in melanocytes (2, 52), and specific binding of MITF was demonstrated at the CATGTG hexametric motif in the promoter region of the tyrosinase gene.

Four mutant alleles, *mi*, Mi^{wh}, mi^{ew}, and Mi^{or}, are known to have mutations in the basic domain (20, 43). One of four arginines (214 to 217) is depleted in the *mi* mutant allele; a point mutation of the nucleotide results in an amino acid change from isoleucine to asparagine at 212 in the Mi^{wh} mutant allele. In the mi^{ew} mutant allele, 75 bp of intragenic deletion results in a lack of 25 amino acids from 187 to 212 and most of the basic domain is missing. In the Mi^{or} mutant allele, the arginine at 216 is changed to lysine. Biochemical analysis by means of electrophoretic gel mobility shift assay showed that MITFs encoded by these mutant alleles (*mi*-MITF, Mi^{wh}-MITF, mi^{ew}-MITF, and Mi^{or}-MITF) not only were incapable of binding to DNA as homodimers (19, 31) but also interfered with the DNA binding of wild-type MITF, TFE3, and another bHLH-ZIP protein in vitro. Although a dominant negative effect is demonstrated in vitro, it has not been clear whether these mutant MITFs have a dominant negative effect on transcriptional activation in vivo. Homozygous *mi*/*mi*, Mi^{wh}/Mi^{wh}, mi^{ew}/mi^{ew}, and Mi^{or}/Mi^{or} mice lack melanocytes, and their coat color is white (15, 40). The dominant negative phenotype of heterozygous $Mi^{wh}/+$ and $Mi^{or}/+$ mice was much more appar-

* Corresponding author. Mailing address: Department of Pathology, Osaka University Medical School, 2-2 Yamada-oka, Suita, Osaka 565, Japan. Phone: 81-06-879-3722. Fax: 81-06-879-3729. Electronic mail address: nomura@patho.med.osaka-u.ac.jp.

ent than that of heterozygous *mi*/+ and *mi*^{ew}/+ mice. The coat color is apparently lighter in *Mi*^{wh}/+ and *Mi*^{or}/+ mice but not in *mi*/+ and *mi*^{ew}/+ mice (15, 40).

Protein localized in the nucleus frequently contains specific nuclear localization signal (NLS) that is required for active transportation across the nuclear envelope (9, 11). The structure component of nuclear envelope includes the double membrane, the nuclear pore complex, and the nuclear lamina. NLS is recognized by NLS-binding protein, which functions as an adapter molecule between the nuclear protein and the nuclear pore complex. Following binding to the nuclear pore complex, the protein is transported through the nuclear pore into the nucleus. A number of NLSs have been identified in various nuclear proteins including bHLH-ZIP transcription factors (11). Viral Jun (v-Jun) is one of the nuclear proteins whose NLS is identified as ASKSRKRKL at positions 245 to 253 (6). The amino acid sequence in the basic domain of MITF contains a motif similar to NLS of v-Jun, i.e., NLIERRRRFNIN at positions 210 to 221, which is considered to be a putative NLS of MITF.

There is a possibility that the discrepancy in phenotype among *mi*/+, *Mi*^{wh}/+, *mi*^{ew}/+, and *Mi*^{or}/+ mice is attributable to the difference in their nuclear localization potentials. In the present study, we compared the nuclear localization potential among wild-type MITF and mutant MITFs. Furthermore, we examined whether mutant MITFs have a dominant negative effect on transcriptional activation of the tyrosinase promoter in vivo.

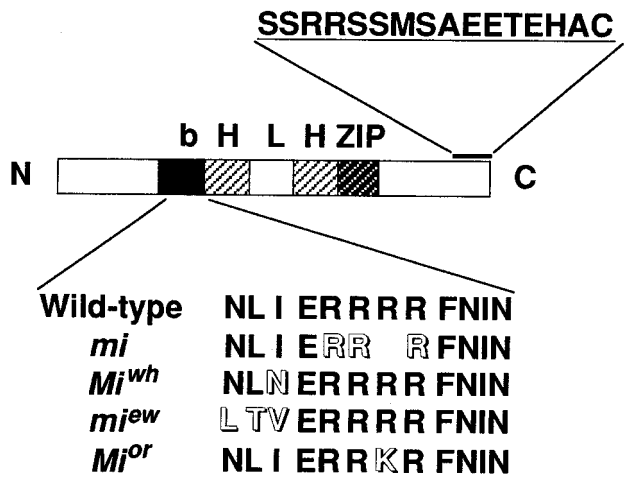

FIG. 1. Structure of MITF. The amino acid sequence of the C-terminal region used for immunization is underlined. Amino acid sequences of the basic domain are also shown. Shown are sequences of the wild-type (amino acids 210 to 221), *mi*-type (amino acids 210 to 220), *Mi*^{wh}-type (amino acids 210 to 221), *mi*^{ew}-type (amino acids 185 to 196), and *Mi*^{or}-type (amino acids 210 to 221) basic domains.

MATERIALS AND METHODS

Plasmid constructs. A cDNA fragment, which contains the entire open reading frame of wild-type MITF (nucleotides 148 to 1422) (31) was subcloned into pGEX3X bacterial expression vector (Pharmacia Biotech, Uppsala, Sweden) which produced glutathione *S*-transferase (GST)–wild-type MITF fusion protein (41). The pGEX3X or pGEX3X–wild-type MITF plasmid was introduced into *Escherichia coli* DH5α cells (Clontech Laboratories, Palo Alto, Calif.). The expression of the GST or GST–wild-type MITF fusion protein was achieved with the addition of the inducer isopropyl-β-D-thiogalactoside (1 mM), and the *E. coli* cells were harvested 2 h later (31). As above, the wild-type MITF cDNA was subcloned into pEF-BOS mammalian expression vector (30) which carried the simian virus 40 (SV40) replication origin and promoter of elongation factor 1α (pEF-BOS-wild-type MITF). The construction of pEF-BOS-*mi*-MITF was as described above, except that the cDNA insert was the reverse transcription-PCR-amplified fragment of the RNA prepared from mast cells of *mi*/*mi* mice. pEF-BOS-*Mi*^{wh}-MITF and pEF-BOS-*Mi*^{or}-MITF were generated by site-directed mutagenesis of pEF-BOS-wild-type MITF. pEF-BOS-*mi*^{ew}-MITF was generated by using PCR, in which oligonucleotide primers are designed in inverted tail-to-tail directions (23). The pSPLucTyr plasmid contained the promoter region of the mouse tyrosinase gene (−329 to +65) (39) cloned into pSPLuc. The luciferase gene subcloned into pSP72 (pSPLuc) was generously provided by K. Nakajima (Osaka University Medical School, Osaka, Japan) (33). pEF-BOS-CNLS-*mi*-MITF and pEF-BOS-NNLS-*mi*-MITF plasmids which contained cDNA encoding the SV40 large-T-antigen NLS (126PKKKRKV112) (25) in the C terminus or N terminus of MITF were generated by using PCR. To generate the Myc-tagged MITF construct, we subcloned the *Sma*I-*Hin*cII fragment of pBS-+/+-MITF (31) into the *Stu*I site of the CS2+ MT expression vector that provides six copies of the Myc epitope tag (EQKLISEEDL) at the N-terminal end of the protein (a gift from A. Suzuki, originally obtained by D. Turner [46]), and the resultant chimeric gene was subcloned into pEF-BOS. A similarly designed influenza virus hemagglutinin (HA)-tagged MITF expression construct encoded a triple N-terminal anti-HA epitope tag (YPYDVPDYA) (a gift from M. Hibi, originally obtained by T. Deng [8]) fused to full-length MITF. Nucleotide sequences of these plasmids were confirmed by dideoxynucleotide sequencing.

Mice, cell culture, DNA transfection, and cotransfection assay. C57BL/6-*mi*/*mi* (*mi*/*mi*) mice, C57BL/6-*Mi*^{wh}/*Mi*^{wh} (*Mi*^{wh}/*Mi*^{wh}) mice, and their normal (+/+) littermates were raised in our laboratory. VGA-9 mice were generated in a previous study (20) and were demonstrated to be the result of the insertional mutation of the mouse vasopressin gene (18) to the *mi* locus. The NIH 3T3 fibroblast cell line and the NRK49F normal rat kidney cell line were obtained from the Japanese Cancer Research Resource Bank (Tokyo, Japan). The 293T human embryonic kidney cell line (12) was kindly provided by D. Baltimore (Rockefeller University, New York, N.Y.). These cell lines were adapted to grow in Dulbecco's modification of Eagle's medium (Flow Laboratories, Irvine, United Kingdom) supplemented with 70 μg of penicillin per ml, 100 μg of streptomycin per ml, and 10% fetal bovine serum (Nippon Bio-Supp Center, Tokyo, Japan) in a humid condition with 5% CO_2 at 37°C. DNA transfection was carried out by the calcium phosphate method as described previously (51). Cotransfection assays were performed according to the method of Yasumoto et al. (52). A pSPLucTyr reporter gene (10 μg) was cotransfected with 5 μg of pEF-BOS-wild-type MITF together with various amounts of mutant MITF constructs indicated in Table 1 and 1 μg of the β-galactosidase expression vector containing the human elongation factor promoter as an internal control. In all cotransfection assays, the total amount of DNA was adjusted to 26 μg/100-mm dish by the addition of a pEF-BOS plasmid DNA. The NIH 3T3 cells were harvested 48 h after the transfection and lysed with 0.1 M potassium phosphate buffer (pH 7.4) containing 1% Triton X-100. Soluble extracts were then assayed for luciferase activity with a luminometer (LB96P; Berthold GmbH, Wildbad, Germany) and for β-galactosidase activity. In each experiment, the luciferase activity was normalized by the β-galactosidase activity and protein concentration, which were then divided by the luciferase activity obtained from cells cotransfected with the pSPLucTyr reporter and pEF-BOS vector (the fold of activation).

Preparation of anti-MITF antibody. To obtain anti-MITF antibody, a synthetic peptide representing the C-terminal region of the MITF (amino acids 404 to 419; 404SSRRSSMSAEETEHAC419, the underlined region in Fig. 1) was conjugated with bovine serum albumin (BSA) and immunized against rabbits. Serum of a rabbit was affinity purified by BSA-coupled resin followed by synthetic peptide-BSA-coupled resin. The affinity-purified anti-MITF antibody was termed MIC4.

Immunocytochemistry. All subsequent steps were carried out at room temperature unless otherwise noted. The cells were fixed 48 h after transfection with 100% methanol twice for 5 min at 4°C and washed with phosphate-buffered saline (PBS; 10 mM sodium phosphate buffer [pH 7.4], 150 mM NaCl) twice for 5 min. The cells were permeabilized by treatment with 0.2% Triton X-100 in PBS for 2 min and washed with PBS four times for 5 min. Then the cells were incubated in 0.3% H_2O_2 in methanol for 30 min to inactivate internal peroxidase, washed with PBS six times for 5 min, and incubated with 1% BSA in PBS for 30 min. Then the cells were incubated with the MIC4 antibody at the protein concentration of 1 μg/ml in PBS containing 0.1% BSA and 0.1% Tween 20 (TBPBS) overnight at 4°C and washed with PBS containing 0.01% Tween 20 four times for 5 min. The cells were incubated with biotin-conjugated goat anti-rabbit immunoglobulin G (IgG) (DAKO A/S, Glostrup, Denmark) in TBPBS for 60 min. Immunoreacted cells were visualized with streptavidin-peroxidase (DAKO) and 0.05% diaminobenzidine–0.02% H_2O_2 solution according to the manufacturer's instructions.

Preparation of cytoplasmic and nuclear extracts for immunoblotting. Cytoplasmic and nuclear extracts were prepared as described by Schreiber et al. (38) with minor modifications. Transfected cells in 100-mm dishes were collected 48 h after transfection and washed with PBS twice by centrifugation at 1,500 × *g* for 10 min at 4°C. Then the cells were resuspended by gentle pipetting in 40 μl of ice-cold buffer A (10 mM HEPES [*N*-2-hydroxyethylpiperazine-*N*′-2-ethanesulfonic acid] [pH 7.9], 10 mM KCl, 1.5 mM $MgCl_2$, 0.1 mM EDTA, 0.1 mM EGTA [ethylene glycol-bis(β-aminoethyl ether)-*N*,*N*,*N*′,*N*′-tetraacetic acid], 1 mM dithiothreitol, 1 mM phenylmethylsulfonyl fluoride [PMSF], 2 μg of pepstatin per ml, 2 μg of leupeptin per ml, 2 μg of antipain per ml, 2 μg of elastatinal per ml).

The cells were allowed to swell on ice for 3 min, and Nonidet P-40 was added to a final concentration of 0.1%. After vigorous vortexing for 10 s, the homogenate was centrifuged at 3,000 rpm for 3 min at 4°C in a high-speed refrigerated microcentrifuge (model MRX-150; Tomy, Tokyo, Japan). The supernatant was used as the cytoplasmic fraction. The pellet was resuspended in 40 μl of ice-cold RIPA buffer (150 mM NaCl, 1% Nonidet P-40, 0.5% sodium deoxycholate, 0.1% sodium dodecyl sulfate [SDS], 50 mM Tris-HCl [pH 7.4], 1 mM PMSF, 2 μg of pepstatin per ml, 2 μg of leupeptin per ml, 2 μg of antipain per ml, 2 μg of elastatinal per ml), disrupted by sonication at maximal power for 10 s at 4°C, and kept on ice for 30 min. The homogenate was centrifuged at 15,000 rpm for 20 min at 4°C. The supernatant was used as the nuclear extract. Cytoplasmic and nuclear fractions of the heart were prepared as described above, except that 1.0 g of dissected tissue was homogenized in 2.0 ml of ice-cold buffer A.

Immunoblotting. Samples were separated by SDS-polyacrylamide gel electrophoresis (SDS-PAGE) and transferred to polyvinylidene difluoride membrane (Immobilon P; Millipore, Bedford, Mass.). The blots were incubated with 5% skim milk in Tris-buffered saline (TBS; 20 mM Tris-HCl [pH 7.4], 150 mM NaCl) overnight at 4°C. Then, the blots were incubated with TBS containing 5% skim milk with the anti-GST antiserum (Santa Cruz Biotechnology, Santa Cruz, Calif.) at a dilution of 1:100 or MIC4 antibody at the protein concentration of 1 μg/ml for 2 h at room temperature. The membrane was washed with TBS containing 0.1% Tween 20 (TTBS) four times for 15 min and was incubated with secondary antibody in TTBS, peroxidase-conjugated goat anti-rabbit IgG (H+L) antibody at a dilution of 1:10,000 (Jackson ImmunoResearch Laboratories, West Grove, Pa.), or peroxidase-conjugated sheep anti-mouse immunoglobulin $F(ab')_2$ fragment at a dilution of 1:3,000 (Amersham, Little Chalfont, Buckinghamshire, England). The membrane was washed with TTBS four times for 15 min, and then the immune complexes were visualized with the enhanced chemiluminescence Western blotting (immunoblotting) detection reagents (Amersham). Then the blots were exposed to Kodak XJB-1 films. The intensity of the signal was quantified by using a densitometer (Molecular Dynamics, Sunnyvale, Calif.). The ratio of the nuclear fraction intensity to the total intensity (nuclear and cytoplasmic fractions) was calculated.

Immunoprecipitation. The 293T cells were transfected with 10 μg each of the appropriate expression constructs indicated in Fig. 6. Forty-eight hours after the transfection, the cytoplasmic extracts were prepared as described above. For the immunoprecipitation, the nuclear extracts were prepared as described by Ron and Harbener (36) with minor modifications. The nuclei were extracted for 30 min at 4°C in buffer B (20 mM HEPES [pH 7.9], 400 mM NaCl, 1 mM EDTA, 1 mM EGTA, 1 mM dithiothreitol, 1 mM PMSF, 2 μg of pepstatin per ml, 2 μg of leupeptin per ml, 2 μg of antipain per ml, 2 μg of elastatinal per ml). The homogenate was subsequently diluted to 200 mM NaCl in the same buffer lacking the salt and centrifuged at 15,000 rpm for 20 min at 4°C. The supernatant was used as the nuclear extract for immunoprecipitation. The cytoplasmic (40 μl) or nuclear (80 μl) extract was incubated with 350 μl of LIP buffer (10 mM HEPES [pH 7.9], 250 mM NaCl, 0.1% Nonidet P-40, 5 mM EDTA, 1 mM PMSF, 2 μg of pepstatin per ml, 2 μg of leupeptin per ml, 2 μg of antipain per ml, 2 μg of elastatinal per ml) and protein G-Sepharose (Pharmacia Biotec) for 1 h at 4°C with gentle rocking and centrifuged at 15,000 rpm for 1 min at 4°C. The supernatant was transferred into a new tube and incubated with the monoclonal antibody directed to the HA epitope (12CA5, provided as ascites fluid; a gift from M. Hibi) and protein G-Sepharose for 2 h on ice in LIP buffer. The immune complex was washed four times with LIP buffer. Samples were resuspended in loading buffer, analyzed on SDS–10% PAGE, and immunoblotted with the anti-Myc tag antibody (the mouse monoclonal antibody 9E10 [Santa Cruz Biotechnology]).

Conjugation of peptides to IgG and microinjections. The sequences of three synthetic peptides for microinjection assay are shown in Fig. 1: wild-type peptide (C-210NLIERRRRFNIN221-GG), *mi*-type peptide (C-210NLIERRRFNIN220-GG), and Mi^{wh}-type peptide (C-210NLNERRRRFNIN221-GG). The terminal C and GG residues represent an extra cysteine for coupling and glyceryl-glycine functioning as a spacer, respectively. These peptides were conjugated to rabbit IgG with *m*-maleimidobenzoic acid *N*-hydroxysuccinimide ester (MBS) by a slight modification of the method described by Lanford et al. (28). IgG was dissolved at the concentration of 6.7 mg/ml in 50 mM sodium phosphate buffer at pH 7.0. MBS dissolved in dimethylformamide (10 mg/ml) was added to the IgG solution to the final concentration of 0.25 mg/ml. The solution was kept for 30 min at room temperature. The MBS-treated IgG was separated from unreacted MBS by gel filtration through a PD10 column (Pharmacia Biotec) and then incubated with 10 mg of synthetic peptide per ml for 5 h. Uncoupled peptide was removed by dialysis against PBS overnight. Microinjections were performed with an Eppendorf 5242 microinjector and 5170 micromanipulator (Eppendorf, Hamburg, Germany) attached to a Nikon inverted phase-contrast microscope (Nikon, Tokyo, Japan). Peptide-IgG conjugates at 3 mg/ml in PBS were injected into the cytoplasm of 200 to 300 NRK49F cells grown on coverslips. The microinjected cells were transferred to fresh Dulbecco's modification of Eagle's medium and incubated in a CO_2 incubator for 2 h at 37°C. The cells were washed with ice-cold PBS and then fixed with formaldehyde. Microinjected rabbit IgG was detected by direct immunofluorescence with goat anti-rabbit IgG antibody conjugated with fluorescein isothiocyanate.

RESULTS

A polyclonal antibody specific for MITF. To obtain anti-MITF antibody, a synthetic peptide representing the C-terminal region of the MITF (the underlined region in Fig. 1) was conjugated with BSA and immunized against rabbits. The obtained antiserum was purified with the column chromatograph containing resin coupled with the synthetic peptide-BSA conjugate. The purified antibody was called MIC4 hereafter. Specificity of the MIC4 antibody was checked by immunoblotting analysis. Extracts of *E. coli* DH5α cells which contained pGEX3X or pGEX3X-wild-type MITF plasmid were purified with the affinity chromatograph containing agarose coupled with glutathione, and the samples were electrophoresed and reacted with the anti-GST antibody. Strong signals were detected at the sizes of 26 and 78 kDa (Fig. 2, lanes 1 and 2), corresponding to the expected size of GST and that of GST–wild-type MITF fusion protein, respectively. In contrast, when the same samples were electrophoresed and reacted with the MIC4 antibody, only the 78-kDa band was detected (Fig. 2, lanes 3 and 4), indicating that GST–wild-type MITF fusion protein was recognizable by the MIC4 antibody. Since the basic domain was remote from the C terminus, which was used as the antigen, the MIC4 antibody bound wild-type MITF, *mi*-MITF, and Mi^{wh}-MITF without significant differences (data not shown).

The specific signal was also obtained with the MIC4 antibody in the nuclear extract prepared from 293T cells transfected with pEF-BOS mammalian expression vector containing wild-type MITF cDNA but not in the nuclear extract prepared from 293T cells transfected with pEF-BOS vector (Fig. 2, lanes 5 and 6). Although the size of the detected signal in SDS-PAGE was slightly larger than expected, the MITF synthesized by the in vitro translation system with rabbit reticulocyte lysate was of comparable size (data not shown). The result indicated that transiently expressed MITF in mammalian cells was specifically recognizable by the MIC4 antibody.

High-level expression of the MITF gene has been reported in the hearts of mice (20, 22). We examined whether the MIC4 antibody recognized the MITF produced in the heart. VGA9 mice whose MITF gene was interrupted by the insertional mutation (20) were used as a negative control. Distinct signal

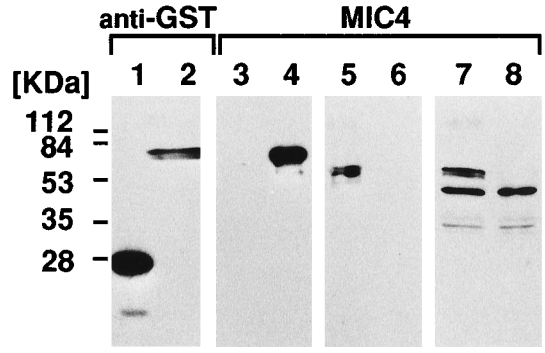

FIG. 2. Demonstration of the specificity of the MIC4 antibody by immunoblotting. Lane 1, extract from *E. coli* DH5α cells which contained pGEX3X; lane 2, extract from *E. coli* DH5α cells which contained pGEX3X-wild-type MITF; lane 3, extract from *E. coli* DH5α cells which contained pGEX3X; lane 4, extract from *E. coli* DH5α cells which contained pGEX3X-wild-type MITF; lane 5, the nuclear extract from 293T cells transfected with pEF-BOS-wild-type MITF; lane 6, the nuclear extract from 293T cells transfected with pEF-BOS vector; lane 7, the heart nuclear extract from +/+ mice; lane 8, the heart nuclear extract from VGA9 mice. Samples were separated by SDS–15% PAGE. Immunoblotting analysis was carried out with the anti-GST antibody (lanes 1 and 2) or with the MIC4 antibody (lanes 3 to 8). Molecular mass is indicated on the left.

was detected in the heart nuclear extract from +/+ mice (Fig. 2, lane 7) but not in the heart nuclear extract from VGA9 mice (Fig. 2, lane 8). The size of signal was comparable to that of 293T cells transfected with pEF-BOS-wild-type MITF (Fig. 2, lane 5).

Subcellular localization of wild-type and mutant MITFs. To examine subcellular localization of MITF, NIH 3T3 and 293T cells were transfected with pEF-BOS, pEF-BOS containing wild-type MITF cDNA, pEF-BOS containing *mi*-MITF cDNA, or pEF-BOS containing Mi^{wh}-MITF cDNA. Transfected cells were stained with the MIC4 antibody 48 h after transfection. When NIH 3T3 and 293T cells were transfected with pEF-BOS-wild-type MITF, a strong signal was observed in the nuclei of approximately 20% of the cells (Fig. 3A and E). No signals were detectable in the remaining 80% of NIH 3T3 and 293T cells probably because of the failure of incorporation of DNA. On the other hand, a strong signal was predominantly localized in the cytoplasm of approximately 20% of NIH 3T3 and 293T cells transfected with pEF-BOS-*mi*-MITF (Fig. 3B and F). These results indicated that wild-type MITF produced by NIH 3T3 and 293T cells was normally transported into the nuclei and that *mi*-MITF was defective in the nuclear translocation. In the NIH 3T3 and 293T cells transfected with pEF-BOS-Mi^{wh}-MITF, the signal was detected in the nuclei of approximately 20% of the cells (Fig. 3C and G), demonstrating the normal nuclear translocation of Mi^{wh}-MITF. When pEF-BOS vector was transfected, no signals were detectable in both NIH 3T3 and 293T cells (Fig. 3D and H), indicating that the MIC4 antibody specifically bound wild-type and mutant MITFs produced within these cultured cells and that the significant amount of endogenous MITF was produced by neither NIH 3T3 nor 293T cells.

The distribution of wild-type and mutant MITFs in NIH 3T3 cells was also examined and quantified by immunoblotting analysis. Strong signal was obtained in the nuclear extract prepared from the cells transfected with pEF-BOS-wild-type MITF but not in the cytoplasmic fraction of the same cells (Fig. 4A, lanes 1 and 2). The size of the immunoreactive protein was identical to that shown in Fig. 2. By quantitative analysis with the densitometer, more than 99% of wild-type MITF was localized in the nuclear fraction. In contrast, only 32% of *mi*-MITF was localized in the nuclear fraction, and the remaining 68% was detected in the cytoplasmic fraction. In the case of Mi^{wh}-MITF, more than 99% was localized in the nuclear fraction. Comparable results were obtained when 293T cells were used instead of NIH 3T3 cells (Fig. 4B).

Functional analysis of putative NLS of MITFs. To examine whether the putative NLS sequences in the basic domain of wild-type, *mi*, and Mi^{wh}-MITFs are biologically functional, synthetic peptides composed of 11 (*mi* type) or 12 (wild type and Mi^{wh} type) amino acids were conjugated with rabbit IgG and injected into NRK49F cells. The amino acid sequences of the injected peptides are shown in Fig. 1. One to three picograms of conjugates was injected into the cytoplasm. Two hours after injection, the localization of peptide-IgG conjugate was determined under the fluorescence microscope. When the wild-type peptide-IgG conjugate was injected, strong signal was detected in the nuclei (Fig. 5A). In contrast, the *mi*-type peptide-IgG conjugate was detected only in the cytoplasm of injected cells (Fig. 5B). The Mi^{wh}-type peptide-IgG conjugate was detected in the nuclei as in the case of wild-type peptide-IgG conjugate (Fig. 5C). When unconjugated IgG was injected, the signal was detected only in the cytoplasm (data not shown). These results indicated that the *mi*-type peptide-IgG conjugate was deficient in the nuclear transportation potential compared with the wild-type and Mi^{wh}-type peptide-IgG conjugates.

Dominant negative effect of nucleus-localized *mi*-MITF on transcriptional activation of the tyrosinase promoter by wild-type MITF. It has been reported that *mi*-MITF and Mi^{wh}-MITF had inhibitory effects on the DNA binding activities of wild-type MITF (19). To examine the dominant negative effect of mutant MITFs on transactivation of the tyrosinase promoter by wild-type MITF, the cotransfection assay was carried out. The NIH 3T3 cells were cotransfected with pEF-BOS-wild-type MITF and pSPLucTyr plasmids. Forty-eight hours after transfection, cells were harvested and the luciferase activity was examined. When the luciferase activity was compared with that of pEF-BOS and pSPLucTyr by cotransfection assay, fivefold activation by wild-type MITF was observed (Table 1). By the addition of pEF-BOS-Mi^{wh}-MITF to the system, the tyrosinase promoter activity was dramatically decreased, which was at least fivefold less compared with that by wild-type MITF. When pEF-BOS-*mi*-MITF was tested, a slight decrease of tyrosinase promoter activity was observed, but the inhibitory effect was much lower compared with that of pEF-BOS-Mi^{wh}-MITF.

To examine whether the smaller inhibitory effect of *mi*-MITF was due to the lower concentration of MITF in the nucleus, pEF-BOS-CNLS-*mi*-MITF and pEF-BOS-NNLS-*mi*-MITF plasmids which contained cDNA encoding the SV40 large-T-antigen NLS (25) in the C terminus or N terminus of MITF were constructed and used for cotransfection assay. When NIH 3T3 cells were transfected with pEF-BOS-CNLS-*mi*-MITF plasmid, more than 80% of CNLS-*mi*-MITF was demonstrated to be localized in the nucleus by immunoblotting with the MIC4 antibody (data not shown). Comparable results were obtained when pEF-BOS-NNLS-*mi*-MITF plasmid was used instead of pEF-BOS-CNLS-*mi*-MITF plasmid. In cotransfection assays, it was demonstrated that the transactivation by wild-type MITF was repressed following cotransfection with either pEF-BOS-CNLS-*mi*-MITF or pEF-BOS-NNLS-*mi*-MITF expression vector in a dose-dependent manner (Table 1). These results indicated that both Mi^{wh}-MITF and *mi*-MITF had dominant negative effects on transactivation of tyrosinase promoter by wild-type MITF. However, because of the defectiveness of *mi*-MITF in the nuclear transportation, *mi*-MITF had a recessive negative effect on transactivation of the tyrosinase promoter.

***mi*-MITF interacted with wild-type MITF in the cytoplasm and inhibited nuclear translocation of wild-type MITF.** MITF was considered to function as homodimers or heterodimers with other bHLH-ZIP proteins (19, 31, 43). To investigate whether the dimerization of MITF occurs in the cytoplasm or nuclei, we subcloned the coding region of wild-type MITF downstream of the Myc epitope in pEF-BOS mammalian expression vector (pEF-BOS-Myc-wild-type MITF). We also constructed the coding region of *mi*-MITF downstream of the influenza virus HA epitope (pEF-BOS-HA-*mi*-MITF). Subconfluent 293T cells were cotransfected with these expression vectors either singly or in combination. Cytoplasmic and nuclear extracts were prepared under nonionic detergent conditions from transfected cells and subjected to direct immunoblotting with the MIC4 antibody (Fig. 6A) or immunoprecipitated with anti-HA-tag antibody (12CA5) and then immunoblotted with anti-Myc-tag antibody (9E10) (Fig. 6B). When the cells were transfected with pEF-BOS-Myc-wild-type MITF alone, the MIC4 antibody detected the pEF-BOS-Myc-wild-type MITF gene product ($MITF^{Myc}$) only in the nuclear fraction by direct immunoblotting (Fig. 6, lane 2). The same subcellular distribution pattern was obtained by the appearance of $MITF^{Myc}$ when

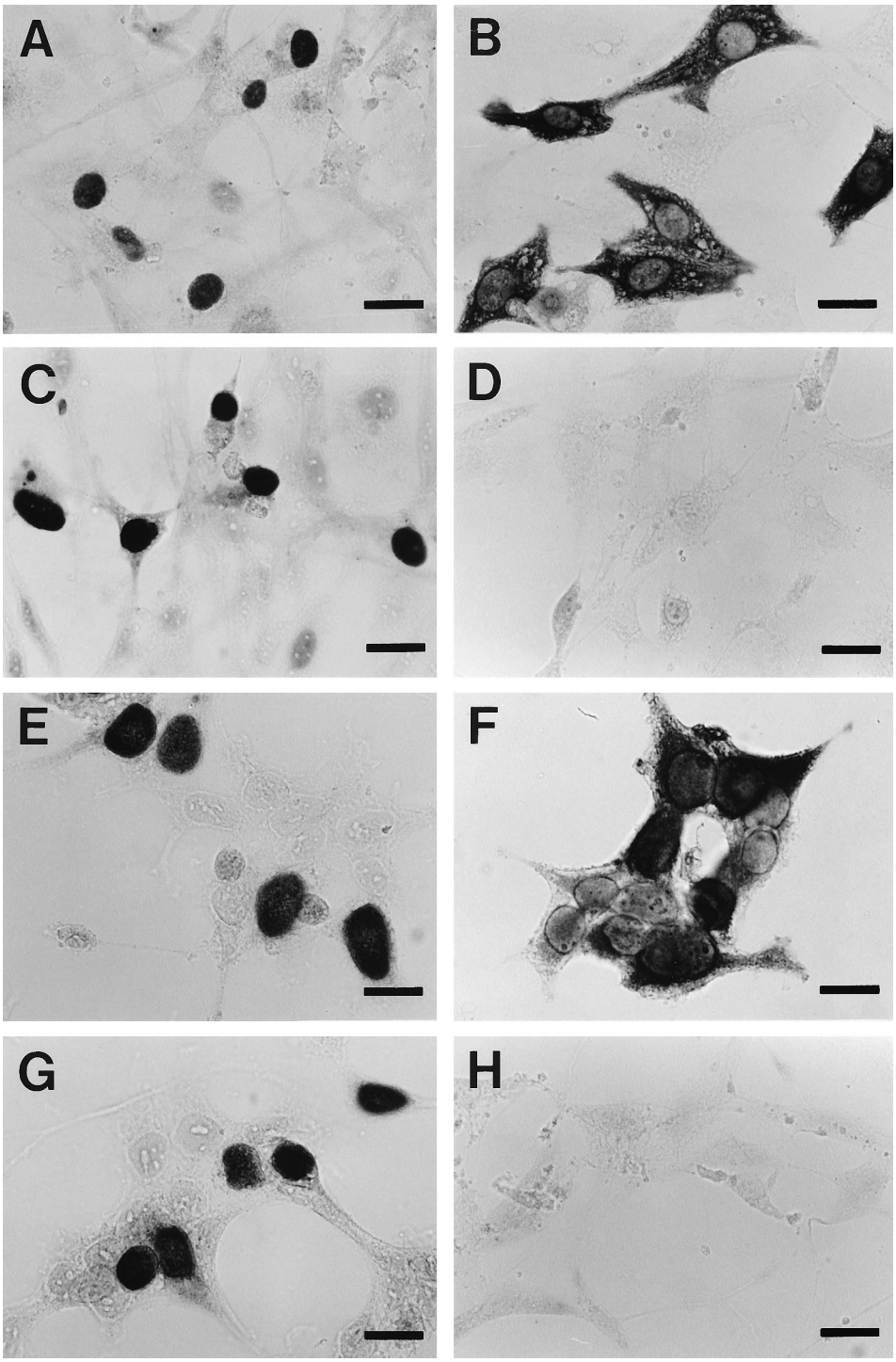

FIG. 3. Subcellular localization of wild-type MITF, *mi*-MITF, and Mi^{wh}-MITF demonstrated by immunocytochemistry. (A) NIH 3T3 cells transfected with pEF-BOS-wild-type MITF; (B) NIH 3T3 cells transfected with pEF-BOS-*mi*-MITF; (C) NIH 3T3 cells transfected with pEF-BOS-Mi^{wh}-MITF; (D) NIH 3T3 cells transfected with pEF-BOS; (E) 293T cells transfected with pEF-BOS-wild-type MITF; (F) 293T cells transfected with pEF-BOS-*mi*-MITF; (G) 293T cells transfected with pEF-BOS-Mi^{wh}-MITF; (H) 293T cells transfected with pEF-BOS. Transfected cells were stained with the MIC4 antibody 48 h after transfection. Scale bars = 10 μm.

the same extracts were immunoprecipitated by anti-Myc-tag antibody (data not shown). These results indicated that epitope-tagged $MITF^{Myc}$ had the same nuclear localization potential as nontagged wild-type MITF. No detectable signal of MITF except that obtained from extracts of cells transfected with pEF-BOS vector alone (Fig. 6, lanes 11 and 12) was obtained when the cytoplasmic and nuclear extracts were immunoprecipitated by anti-HA-tag antibody and immunoblotted with anti-Myc-tag antibody (Fig. 6, lanes 7 and 8). Whereas 293T cells were cotransfected with pEF-BOS-Myc-wild-type

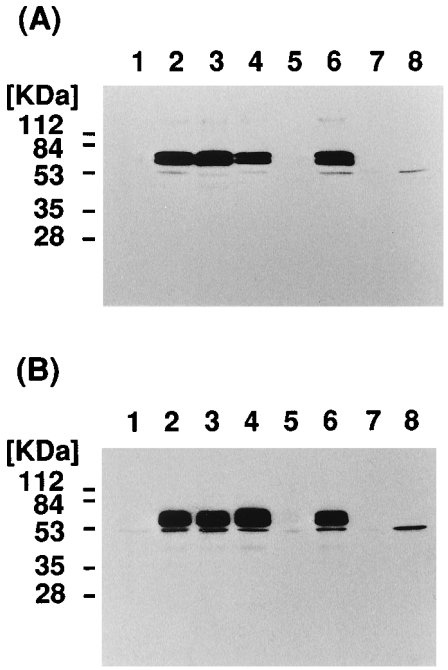

FIG. 4. Subcellular localization of wild-type MITF, *mi*-MITF, and Mi^{wh}-MITF determined by immunoblotting analysis. (A) Cytoplasmic and nuclear extracts were obtained from NIH 3T3 cells; (B) cytoplasmic and nuclear extracts were obtained from 293T cells. Lanes 1, the cytoplasmic extract from cells transfected with pEF-BOS-wild-type MITF; lanes 2, the nuclear extract from cells transfected with pEF-BOS-wild-type MITF; lanes 3, the cytoplasmic extract from cells transfected with pEF-BOS-*mi*-MITF; lanes 4, the nuclear extract from cells transfected with pEF-BOS-*mi*-MITF; lanes 5, the cytoplasmic extract from cells transfected with pEF-BOS-Mi^{wh}-MITF; lanes 6, the nuclear extract from cells transfected with pEF-BOS-Mi^{wh}-MITF; lanes 7, the cytoplasmic extract from cells transfected with pEF-BOS; lanes 8, the nuclear extract from cells transfected with pEF-BOS. Samples were separated on an SDS–15% PAGE gel. Immunoblotting analysis was carried out with the MIC4 antibody. Molecular mass is indicated on the left.

MITF and pEF-BOS-HA-*mi*-MITF, a strong anti-HA-tag antibody-immunoprecipitable and anti-Myc-tag antibody-reactive band was obtained only in the cytoplasmic fraction (Fig. 6, lane 9). When the same extracts were analyzed on direct immunoblotting with the MIC4 antibody, we observed a strong signal of $MITF^{Myc}$ in both the cytoplasmic and the nuclear extracts (Fig. 6, lanes 3 and 4) in the same position as anti-HA-tag antibody-immunoprecipitable and anti-Myc-tag antibody-reactive band. Therefore, it was demonstrable that the signal was derived from $MITF^{Myc}$. On the other hand, pEF-

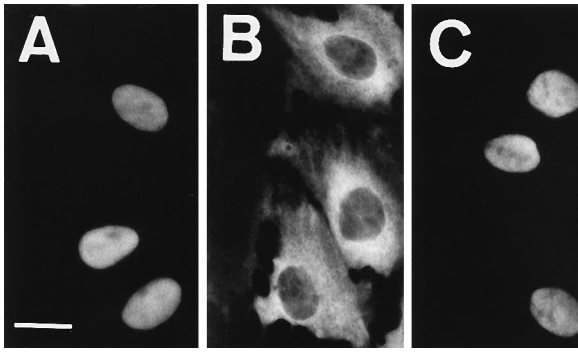

FIG. 5. Nuclear translocation of rabbit IgG mediated by synthetic peptides, a part of the basic domain of MITFs. (A) NRK49F cells microinjected with the wild-type peptide-IgG conjugate; (B) NRK49F cells microinjected with the *mi*-type peptide-IgG conjugate; (C) NRK49F cells microinjected with the Mi^{wh}-type peptide-IgG conjugate. Microinjected NRK49F cells were stained with the fluorescein isothiocyanate-labeled anti-rabbit IgG antibody 2 h after injection. Amino acid sequences of three peptides are shown in Fig. 1. Scale bar = 5 μm.

TABLE 1. Dominant negative effect of mutant MITFs on transactivation of the tyrosinase promoter by wild-type MITF

Cotransfected DNA	Amount of cotransfected DNA (μg)	Activation[a] (fold)
None		5.11 ± 0.16
pEF-BOS-Mi^{wh}-MITF	2.5	1.16 ± 0.03[b]
	5.0	0.83 ± 0.04[b]
	10.0	0.49 ± 0.05[b]
pEF-BOS-*mi*-MITF	2.5	4.19 ± 0.27
	5.0	3.95 ± 0.39
	10.0	2.38 ± 0.41
pEF-BOS-NNLS-*mi*-MITF	2.5	3.01 ± 0.21
	5.0	2.62 ± 0.14
	10.0	1.77 ± 0.12[b]
pEF-BOS-CNLS-*mi*-MITF	2.5	2.85 ± 0.37
	5.0	2.52 ± 0.12
	10.0	1.57 ± 0.13[b]

[a] The luciferase activity was normalized to the β-galactosidase activity and protein concentration, which were divided by the luciferase activity obtained from cells cotransfected with the pSPLucTyr reporter and pEF-BOS (the fold of activation). Each value is the mean ± the standard error.

[b] P is <0.02 by the t test compared with the value for no cotransfected DNA (5.11 ± 0.16).

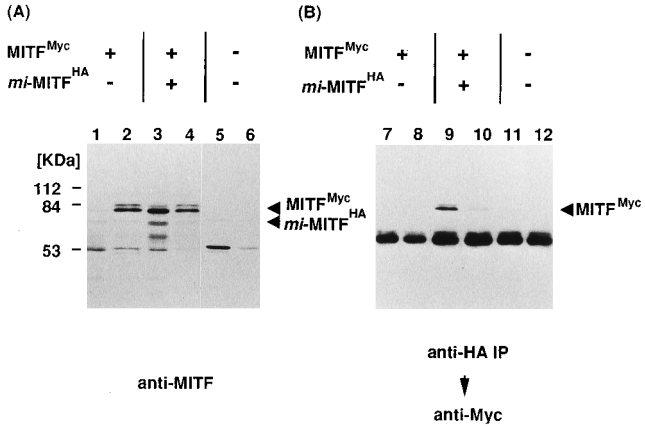

FIG. 6. Interaction between wild-type MITF and *mi*-MITF occurred in the cytoplasm. The cytoplasmic and nuclear extracts were obtained from transfected 293T cells under nonionic detergent conditions for immunoprecipitation as described in Materials and Methods. (A) Direct immunoblotting with the MIC4 antibody of extracts from transfected 293T cells. Samples were separated by SDS–10% PAGE. The positions of migration of the pEF-BOS-Myc-wild-type MITF gene product ($MITF^{Myc}$) and the pEF-BOS-HA-*mi*-MITF gene product (*mi*-$MITF^{HA}$) are indicated by arrowheads on the right. (B) Each extract from the transfected cells was first immunoprecipitated with anti-HA-tag antibody (12CA5). Immunoprecipitated materials were resuspended, and immunoblotting analysis was carried out with anti-Myc-tag antibody (9E10). Samples were separated on an SDS–10% PAGE gel. The position of migration of $MITF^{Myc}$ is indicated by an arrowhead on the right. Lanes 1 and 7, the cytoplasmic extract from cells transfected with pEF-BOS-Myc-wild-type MITF alone; lanes 2 and 8, the nuclear extract from cells transfected with pEF-BOS-Myc-wild-type MITF alone; lanes 3 and 9, the cytoplasmic extract from cells cotransfected with pEF-BOS-Myc-wild-type MITF and pEF-BOS-HA-*mi*-MITF; lanes 4 and 10, the nuclear extract from cells cotransfected with pEF-BOS-Myc-wild-type MITF and pEF-BOS-HA-*mi*-MITF; lanes 5 and 11, the cytoplasmic extract from cells transfected with pEF-BOS plasmid; lanes 6 and 12, the nuclear extract from cells transfected with pEF-BOS plasmid. Molecular mass is indicated on the left.

TABLE 2. Comparison of amino acid sequences of putative NLSs in the MITF-related proteins and v-Jun

Protein	Sequence
MITF	NLIERRRRFNIN
TFE3	NLIERRRRFNIN
TFEB	NLIERRRRFNIN
TFEC	NLIERRRRYNIN
v-Jun	ASKSRKRKL

BOS-HA-*mi*-MITF gene product (*mi*-MITF^{HA}) was detectable only in the cytoplasmic extracts by direct immunoblotting with the MIC4 antibody (Fig. 6, lane 3). When pEF-BOS-Myc-wild-type MITF-transfected cells were mixed with pEF-BOS-HA-*mi*-MITF-transfected cells, and the extracts were prepared from the mixture of independently transfected cells, no anti-HA-tag antibody-immunoprecipitable and anti-Myc-tag antibody-reactive signal was detected (data not shown). These results indicated the possibility that the interaction between *mi*-MITF and wild-type MITF occurred in the cytoplasm and that *mi*-MITF had also an inhibitory effect on nuclear localization potential of wild-type MITF.

Nuclear localization potentials of other mutant MITFs which carry mutations in the basic domain. Our data showed that peptides which contained a part of the basic domain functioned as a NLS of MITF (Fig. 5). This region of MITF was conserved among other bHLH-ZIP transcription factors, TFE3, TFEB, and TFEC (1, 4, 53) (Table 2). It was also reported that other mutant MITFs, *mi*^{ew} and *Mi*^{or}, carried mutations in this basic domain. Nucleotide sequence encoding *mi*^{ew}-MITF showed an internal deletion of 75 bp which results in a lack of 25 amino acids from 187 to 212, and a nucleotide point mutation in *Mi*^{or} results in amino acid substitution of arginine with lysine at 216 (Fig. 1). To examine the subcellular localization of these mutant MITFs, 293T cells were transfected with pEF-BOS-*mi*^{ew}-MITF or pEF-BOS-*Mi*^{or}-MITF, and immunoblotting with the MIC4 antibody was carried out. A strong signal of *Mi*^{or}-MITF was detected in the nuclear fraction (Fig. 7, lane 4), but signal was not detectable in the cytoplasmic fraction prepared from cells transfected with pEF-BOS-*Mi*^{or}-MITF (Fig. 7, lane 3). On the other hand, approximately 40% of *mi*^{ew}-MITF remained in the cytoplasmic fraction prepared from cells transfected with pEF-BOS-*mi*^{ew}-MITF (Fig. 7, lane 1). These results indicated that the nuclear localization potential of *Mi*^{or}-MITF was normal but that *mi*^{ew}-MITF was impaired as in the case of *mi*-MITF (Fig. 7, lanes 5 and 6).

DISCUSSION

We produced the MIC4 antibody that recognized the murine MITF. NIH 3T3 or 293T cells were transfected with the plasmid containing the cDNA of various mutant MITFs which carried mutations in the basic domain. Subcellular localization of MITFs produced by transfected cells was determined by immunocytochemistry or immunoblotting with the MIC4 antibody. Wild-type MITF, *Mi*^{wh}-MITF, and *Mi*^{or}-MITF appear to translocate to the nucleus, but *mi*-MITF and *mi*^{ew}-MITF appear to have a defect in the nuclear translocation. Our results indicated that the deficient nuclear translocation of *mi*-MITF and *mi*^{ew}-MITF may be attributable to the mutation in the basic domain.

However, significant amounts of *mi*-MITF and *mi*^{ew}-MITF were present in the nucleus of 293T cells transfected with the plasmid containing each cDNA, respectively. Some explanations may be possible. (i) Other NLSs may be present in the MITF molecule. Some nuclear proteins such as polyomavirus large T antigen (35), *Saccharomyces cerevisiae* ribosomal protein L29 (47), *S. cerevisiae* MATα2 (16, 17), influenza virus NS1 (14), the core protein of hepatitis C virus (5), and the glucocorticoid receptor (34) contain more than two NLSs. Some *mi*-MITF and *mi*^{ew}-MITF molecules may translocate to the nucleus by using other NLSs. (ii) The amount of MITF produced in the transfected cells may be too abundant compared with the amount of physiologically produced MITF. A portion of excess *mi*-MITF or *mi*^{ew}-MITF could diffuse into the nucleus in 48 h. However, we do not consider that the physiological amount of *mi*-MITF and *mi*^{ew}-MITF may diffuse into the nucleus.

The peptides containing a part of the basic domain (210NLI ERRRRFNIN221) were conjugated with rabbit IgG and injected into the cytoplasm of NRK49F cells. The conjugates of rabbit IgG with the wild-type or *Mi*^{wh}-type peptide were detected only in the nucleus, but the conjugates with the *mi*-type peptide were detectable only in the cytoplasm. This result is consistent with the result obtained by immunoblotting and immunocytochemistry and clearly indicates that the amino acid sequence of this portion in the basic domain of MITF functions as an NLS. It was also demonstrated that the nuclear translocation ability was completely lost by a deletion of an arginine residue. The present result is consistent with a previous study (6) that found that a series of four basic amino acids is essential for the nuclear translocation in the v-Jun protein (Table 2). In the case of *mi*^{ew}-MITF, lacking 25 amino acids from 187 to 212, the mutation removes all but five (213ERRRR217) amino acids in the basic domain (43). It was reported that there are two NLSs in the human c-Myc protein having a bHLH-ZIP structure (7), residues 320 to 328 (320PAAKRVKLD328; peptide M1) and residues 364 to 374 (364RQRRNELKRSP374; peptide M2). The amino acid sequence from 210 to 221 (210NLIERRRRFNIN221) corresponds to the M2 region, and the deleted amino acid sequence in *mi*^{ew}-MITF (187 to 212) involves a sequence similar to that of the M1 region of c-Myc. Therefore, we consider that residues 210 to 221 function as the NLS of MITF and additional NLS is present within the region from 187 to 212. The basic domain of MITF is highly conserved among other bHLH-ZIP transcription factors, TFE3, TFEB, and TFEC (1, 4, 53) (Table 2). It is possible to speculate that

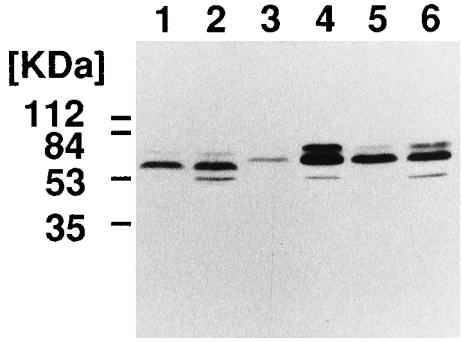

FIG. 7. Subcellular localization of *mi*^{ew}-MITF and *Mi*^{or}-MITF. The cytoplasmic and nuclear extracts were obtained from 293T cells. Lane 1, the cytoplasmic extract from cells transfected with pEF-BOS-*mi*^{ew}-MITF; lane 2, the nuclear extract from cells transfected with pEF-BOS-*mi*^{ew}-MITF; lane 3, the cytoplasmic extract from cells transfected with pEF-BOS-*Mi*^{or}-MITF; lane 4, the nuclear extract from cells transfected with pEF-BOS-*Mi*^{or}-MITF; lane 5, the cytoplasmic extract from cells transfected with pEF-BOS-*mi*-MITF; lane 6, the nuclear extract from cells transfected with pEF-BOS-*mi*-MITF. Samples were separated on an SDS–15% PAGE gel. Immunoblotting analysis was carried out with the MIC4 antibody. Molecular mass is indicated on the left.

the NLSs of these bHLH-ZIP proteins may locate at this region as well.

Homozygous *mi*/*mi*, Mi^{wh}/Mi^{wh}, mi^{ew}/mi^{ew}, and Mi^{or}/Mi^{or} mice lack melanocytes, and their coats are white (15, 40). The phenotype could be explained by the dominant negative effect of mutant MITFs encoded by these mutant alleles on DNA binding. These mutant MITFs interfere with the DNA binding of wild-type MITF, TFE3, and another bHLH-ZIP protein (19). Despite the dominant negative effect on DNA binding, a discrepancy of phenotype among these heterozygous mice is observed. The coat color is apparently lighter in $Mi^{wh}/+$ and $Mi^{or}/+$ mice but not in *mi*/+ and $mi^{ew}/+$ mice (15, 40). Therefore, the dominant negative effect of the Mi^{wh} and Mi^{or} mutant allele is much more remarkable than that of the *mi* and mi^{ew} mutant allele. MITF is considered to function as a homodimer or heterodimer with other bHLH-ZIP proteins (19, 31). The different phenotypes of coat color among heterozygous mutant mice may be explained as follows. Since the Mi^{wh}-MITF and Mi^{or}-MITF translocate into the nucleus with the same efficiency as wild-type MITF, dimers between mutant MITF and wild-type MITF and dimers between mutant MITF and other bHLH-ZIP proteins are accumulated in the nucleus. The function of such dimers is considered to be deficient (19), and therefore heterozygous $Mi^{wh}/+$ and $Mi^{or}/+$ mice show abnormal phenotypes. Since our findings indicated that *mi*-MITF and mi^{ew}-MITF showed the depletion of the translocation into the nucleus with neither mutant MITF nor wild-type MITF, the homodimer of wild-type MITF, whose function is normal, selectively accumulated in the nucleus. Even though some amount of wild-type MITF is trapped in the cytoplasm by *mi*-MITF, the amount of wild-type MITF homodimer in the nucleus which is produced by the + allele of *mi*/+ and $mi^{ew}/+$ mice may be enough for pigmentation in hairs during development. In fact, our results showed that Mi^{wh}-MITF had a strong dominant negative effect on transactivation of the tyrosinase promoter by wild-type MITF. On the other hand, an inhibitory effect of *mi*-MITF was much smaller than that of Mi^{wh}-MITF. Since an inhibitory effect of *mi*-MITF was enhanced by conjugation of SV40 large-T-antigen-derived NLS, it was demonstrated that the smaller inhibitory effect of *mi*-MITF was due to the lower concentration of *mi*-MITF in the nucleus. As a result, heterozygous *mi*/+ and $mi^{ew}/+$ mice show an almost normal phenotype because of deficiency in the nuclear localization potential.

Our data from coimmunoprecipitation assay showed that *mi*-MITF interacted with wild-type MITF in the cytoplasm and had an inhibitory effect on nuclear translocation of wild-type MITF. A similar interaction was reported in that a mutant SV40 large T antigen failed to localize normally in the nucleus and interfered with nuclear translocation of another nuclear protein, adenovirus 5 fiber protein (37). The homozygous *mi*/*mi* mice show phenotypes in addition to those of other MITF mutants, osteopetrosis and a decrease in the number of mast cells (10, 26, 29, 48, 49). The reason for additional phenotypes in homozygous *mi*/*mi* mice is still unknown, but we can speculate that *mi*-MITF associates with another protein whose function is indispensable in specific cell types such as osteoclasts and/or mast cells and inhibits the nuclear translocation of the protein. Interallelic complementation observed in doubly heterozygous mi/Mi^{wh} mice shows the phenotype of eyes being larger and slightly more pigmented than those of either *mi* or Mi^{wh} homozygotes alone (21). The phenotype of the mi/Mi^{wh} mice supports our idea that because Mi^{wh}-MITF has normal nuclear localization potential, the complex between Mi^{wh}-MITF and an unknown factor could translocate normally into the nucleus. This possibility suggests that MITF acts as a nuclear transporter of the protein as well as a transcription factor. Since osteopetrosis was observed in both *mi*/*mi* mice and gene-targeted mice in the c-*fos* gene, their abnormalities resembled each other (24, 50), and the distinct NLSs had not yet been identified in the c-*fos* gene product (FOS), we speculate that FOS or FOS-interacting protein (3) is one of the candidates for the partner for MITF in the cytoplasm of osteoclasts. A further study of interaction partners with MITF, affinity, and MITF target genes may help in the elucidation of the biological function of MITF in specific cell types.

Taken together, the present results indicate the presence of a NLS in the DNA binding domain of MITF. Therefore, the different phenotypes of coat color among mutant mice may be explained by differences in the nuclear localization potential of mutant MITFs. The *mi* and mi^{ew} mutant alleles appear to be the first known mutations which result in the loss of nuclear localization potential in transcription factors; these useful mutants may provide us with important knowledge of the differentiation and proliferation of cells during development.

ACKNOWLEDGMENTS

We thank R. Nakata for support in preparing anti-MITF antibody; T. Akira for plasmid constructions; M. Hibi for providing the plasmid for HA epitope-tagging and the 12CA5 antibody; K. Morihana and A. Fukuyama for their excellent technical support; T. Tsujimura, M. Yamamoto, and T. Jippo for helpful discussion; and A. Suzuki for providing various plasmids and encouragement during the course of this work.

This work was supported by grants from the Ministry of Education, Science and Culture; the Ministry of Health and Welfare; the Naito Foundation; and the Motida Memorial Foundation for Medical and Pharmaceutical Research.

REFERENCES

1. **Beckmann, H., L. Su, and T. Kadesch.** 1990. TFE3: a helix-loop-helix protein that activates transcription through the immunoglobulin enhancer μE3 motif. Genes Dev. **4:**167–179.
2. **Bentley, N. J., T. Eisen, and C. R. Goding.** 1994. Melanocyte-specific expression of the human tyrosinase promoter: activation by the microphthalmia gene product and role of the initiator. Mol. Cell. Biol. **14:**7996–8006.
3. **Blanar, M. A., and W. J. Rutter.** 1992. Interaction cloning: identification of helix-loop-helix zipper protein that interacts with c-Fos. Science **256:**1014–1018.
4. **Carr, C. S., and P. A. Sharp.** 1990. A helix-loop-helix protein related to the immunoglobulin E box-binding proteins. Mol. Cell. Biol. **10:**4384–4388.
5. **Chang, S. C., J.-H. Yen, H.-Y. Kang, M.-H. Jang, and M.-F. Chang.** 1994. Nuclear localization signals in the core protein of hepatitis C virus. Biochem. Biophys. Res. Commun. **205:**1284–1290.
6. **Chida, K., and P. K. Vogt.** 1992. Nuclear translocation of viral Jun but not of cellular Jun is cell cycle dependent. Proc. Natl. Acad. Sci. USA **89:**4290–4294.
7. **Dang, C. V., and W. M. F. Lee.** 1988. Identification of the human c-*myc* protein nuclear translocation signal. Mol. Cell. Biol. **8:**4048–4054.
8. **Dérijard, B., M. Hibi, I.-H. Wu, T. Barrett, B. Su, T. Deng, M. Karin, and R. J. Davis.** 1994. JNK1: a protein kinase stimulated by UV light and Ha-Ras that binds and phosphorylates the c-Jun activation domain. Cell **76:**1025–1037.
9. **Dingwall, C., and A. Laskey.** 1991. Nuclear targeting sequences—a consensus? Trends Biochem. Sci. **16:**478–481.
10. **Ebi, Y., Y. Kanakura, T. Jippo-Kanemoto, T. Tsujimura, T. Furitsu, H. Ikeda, S. Adachi, T. Kasugai, S. Nomura, Y. Kanayama, A. Yamatodani, S. Nishikawa, Y. Matsuzawa, and Y. Kitamura.** 1992. Low c-*kit* expression of cultured mast cells of *mi*/*mi* genotype may be involved in their defective responses to fibroblasts that express the ligand for c-*kit*. Blood **80:**1454–1462.
11. **Garcia-Bustos, J., J. Heitman, and M. N. Hall.** 1991. Nuclear protein localization. Biochim. Biophys. Acta **1071:**83–101.
12. **Graham, F. L., J. Smiley, W. C. Russell, and R. Nairn.** 1977. Characteristics of a human cell line transformed by DNA from human adenovirus type 5. J. Gen. Virol. **36:**59–72.
13. **Green, M. C.** 1989. Catalog of mutant genes and polymorphic loci, p. 236–238. *In* M. F. Lyon and A. G. Searle (ed.), Genetic variants and strains of the laboratory mouse. Oxford University Press, Oxford.
14. **Greenspan, D., P. Palese, and M. Krystal.** 1988. Two nuclear location signals in the influenza virus NS1 nonstructural protein. J. Virol. **62:**3020–3026.

15. **Grüneberg, H.** 1953. The relations of microphthalmia and white in the mouse. J. Genet. **51:**359–362.
16. **Hall, M. N., C. Craik, and Y. Hiraoka.** 1990. Homeodomain of yeast repressor α2 contains a nuclear localization signal. Proc. Natl. Acad. Sci. USA **87:** 6954–6958.
17. **Hall, M. N., L. Hereford, and I. Herskowitz.** 1984. Targeting of E. coli β-galactosidase to the nucleus in yeast. Cell **36:**1057–1065.
18. **Hara, Y., J. Battey, and H. Gainer.** 1990. Structure of mouse vasopressin and oxytocin genes. Mol. Brain Res. **8:**319–324.
19. **Hemesath, T. J., E. Steingrímsson, G. McGill, M. J. Hansen, J. Vaught, C. A. Hodgkinson, H. Arnheiter, N. G. Copeland, N. A. Jenkins, and D. E. Fisher.** 1994. *Microphthalmia*, a critical factor in melanocyte development, defines a discrete transcription factor family. Genes Dev. **8:**2770–2780.
20. **Hodgkinson, C. A., K. J. Moore, A. Nakayama, E. Steingrímsson, N. G. Copeland, N. A. Jenkins, and H. Arnheiter.** 1993. Mutations at the mouse microphthalmia locus are associated with defects in a gene encoding a novel basic-helix-loop-helix-zipper protein. Cell **74:**395–404.
21. **Hollander, W. F.** 1968. Complementary alleles at the *mi*-locus in the mice. Genetics **60:**189.
22. **Hughes, M. J., J. B. Lingrel, J. M. Krakowsky, and K. P. Anderson.** 1993. A helix-loop-helix transcription factor-like gene is located at the *mi* locus. J. Biol. Chem. **268:**20687–20690.
23. **Imai, Y., Y. Matsushima, T. Sugimura, and M. Terada.** 1991. A simple and rapid method for generating a deletion by PCR. Nucleic Acids Res. **19:**2785.
24. **Johnson, R. S., B. M. Spiegelman, and V. Papaioannou.** 1992. Pleiotropic effects of a null mutation in the c-*fos* proto-oncogene. Cell **71:**577–586.
25. **Kalderon, D., B. L. Roberts, W. D. Richardson, and A. E. Smith.** 1984. A short amino acid sequence able to specify nuclear location. Cell **39:**499–509.
26. **Kasugai, T., K. Oguri, T. Jippo-Kanemoto, M. Morimoto, A. Yamatodani, K. Yoshida, Y. Ebi, K. Isozaki, H. Tei, T. Tsujimura, S. Nomura, M. Okayama, and Y. Kitamura.** 1993. Deficient differentiation of mast cells in the skin of *mi*/*mi* mice: usefulness of *in situ* hybridization for evaluation of mast cell phenotype. Am. J. Pathol. **143:**1337–1347.
27. **Krakowsky, J. M., R. E. Biossy, J. C. Neumann, and J. B. Lingrel.** 1993. A DNA insertional mutation results in microphthalmia in transgenic mice. Transgenic Res. **2:**14–20.
28. **Lanford, R. E., P. Kanda, and R. C. Kennedy.** 1986. Induction of nuclear transport with a synthetic peptide homologous to the SV40 T antigen transport signal. Cell **46:**575–582.
29. **Marks, S. C., Jr., and D. G. Walker.** 1981. The hematogenous origin of osteoclasts: experimental evidence from osteopetrotic (microphthalmic) mice treated with spleen cells from beige mouse donors. Am. J. Anat. **161:** 1–10.
30. **Mizushima, S., and S. Nagata.** 1990. pEF-BOS, a powerful mammalian expression vector. Nucleic Acids Res. **18:**5322.
31. **Morii, E., K. Takebayashi, H. Motohashi, M. Yamamoto, S. Nomura, and Y. Kitamura.** 1994. Loss of DNA binding ability of the transcription factor encoded by the mutant *mi* locus. Biochem. Biophys. Res. Commun. **205:** 1299–1304.
32. **Motohashi, H., K. Hozawa, T. Oshima, T. Takeuchi, and T. Takasaka.** 1994. Dysgenesis of melanocytes and cochlear dysfunction in mutant microphthalmia (*mi*) mice. Hear. Res. **80:**10–20.
33. **Nakajima, K., T. Kusafuka, T. Takeda, Y. Fujitani, K. Nakae, and T. Hirano.** 1993. Identification of a novel interleukin-6 response element containing an Ets-binding site and a CRE-like site in the *junB* promoter. Mol. Cell. Biol. **13:**3027–3041.
34. **Picard, D., and K. R. Yamamoto.** 1987. Two signals mediate hormone-dependent nuclear localization of the glucocorticoid receptor. EMBO J. **6:** 3333–3340.
35. **Richardson, W. D., B. L. Roberts, and A. E. Smith.** 1986. Nuclear location signals in polyoma virus large-T. Cell **44:**77–85.
36. **Ron, D., and J. F. Harbener.** 1992. CHOP, a novel developmentally regulated nuclear protein that dimerizes with transcription factors C/EBP and LAP and functions as a dominant-negative inhibitor of gene transcription. Genes Dev. **6:**439–453.
37. **Schneider, J., C. Schindewolf, K. van Zee, and E. Fanning.** 1988. A mutant SV40 large T antigen interferes with nuclear localization of a heterologous protein. Cell **54:**117–125.
38. **Schreiber, E., P. Matthias, M. M. Müller, and W. Schaffner.** 1989. Rapid detection of octamer binding proteins with 'mini-extracts', prepared from a small number of cells. Nucleic Acids Res. **17:**6419.
39. **Shibahara, S., S. Okinaga, Y. Tomita, A. Takeda, H. Yamamoto, M. Sato, and T. Takeuchi.** 1990. A point mutation in the tyrosinase gene of BALB/c albino mouse causing the cysteine→serine substitution at position 85. Eur. J. Biochem. **189:**455–461.
40. **Silvers, W. K.** 1979. The coat colors of mice: a model for mammalian gene action and interaction, p. 268–291. Springer-Verlag, New York.
41. **Smith, D. B., and K. S. Johnson.** 1988. Single-step purification of polypeptides expressed in *Escherichia coli* as fusions with glutathione *S*-transferase. Gene **67:**31–40.
42. **Stechschulte, D. J., R. Sharma, K. N. Dileepan, K. M. Simpson, N. Aggarwal, J. Clancy, Jr., and R. L. Jilka.** 1987. Effect of the mi allele on mast cells, basophils, natural killer cells, and osteoclasts in C57Bl/6J mice. J. Cell. Physiol. **132:**565–570.
43. **Steingrímsson, E., K. J. Moore, M. L. Lamoreux, A. R. Ferré-D'Amaré, S. K. Burley, D. C. S. Zimring, L. C. Skow, C. A. Hodgkinson, H. Arnheiter, N. G. Copeland, and N. A. Jenkins.** 1994. Molecular basis of mouse *microphthalmia* (*mi*) mutations helps explain their developmental and phenotypic consequences. Nature (London) Genet. **8:**256–263.
44. **Stevens, J., and J. F. Loutit.** 1982. Mast cells in spotted mutant mice (*W Ph mi*). Proc. R. Soc. Lond. Ser. B. **215:**405–409.
45. **Tachibana, M., L. A. Perez-Jurado, A. Nakayama, C. A. Hodgkinson, X. Li, M. Schneider, T. Miki, J. Fex, U. Francke, and H. Arnheiter.** 1994. Cloning of *MITF*, the human homolog of the mouse *microphthalmia* gene and assignment to chromosome 3p14.1-p12.3. Hum. Mol. Genet. **3:**553–557.
46. **Turner, D. L., and H. Weintraub.** 1994. Expression of achaete-scute homolog 3 in *Xenopus* embryos converts ectodermal cells to a neural fate. Genes Dev. **8:**1434–1447.
47. **Underwood, M. R., and H. M. Fried.** 1990. Characterization of nuclear localization sequences derived from yeast ribosomal protein L29. EMBO J. **9:**91–100.
48. **Walker, D. G.** 1975. Bone resorption restored in osteopetrotic mice by transplants of normal bone marrow and spleen cells. Science **190:**784–785.
49. **Walker, D. G.** 1975. Spleen cells transmit osteopetrosis in mice. Science **190:** 785–787.
50. **Wang, Z.-Q., C. Ovitt, A. E. Grigoriadis, U. Möhle-Steinlein, U. Rüther, and E. F. Wagner.** 1992. Bone and haematopoietic defects in mice lacking c-*fos*. Nature (London) **360:**741–745.
51. **Wigler, M., A. Pellicer, S. Silverstein, R. Axel, G. Urlaub, and L. Chasin.** 1979. DNA-mediated transfer of the adenine phospholibosiltransferase locus into mammalian cells. Proc. Natl. Acad. Sci. USA **76:**1373–1376.
52. **Yasumoto, K., K. Yokoyama, K. Shibata, Y. Tomita, and S. Shibahara.** 1994. Microphthalmia-associated transcription factor as a regulator for melanocyte-specific transcription of the human tyrosinase gene. Mol. Cell. Biol. **14:** 8058–8070.
53. **Zhao, G.-Q., Q. Zhao, X. Zhou, M. Mattei, and B. De Crombrugghe.** 1993. TFEC, a basic helix-loop-helix protein, forms heterodimers with TFE3 and inhibits TFE3-dependent transcription activation. Mol. Cell. Biol. **13:**4505–4512.